# Ebullition Controls on $CH_4$ Emissions in an Urban, Eutrophic River: A Potential Time-Scale Bias in Determining the Aquatic $CH_4$ Flux

Shu Chen, Dongqi Wang,* Yan Ding, Zhongjie Yu, Lijie Liu, Yu Li, Dong Yang, Yingyuan Gao, Haowen Tian, Rui Cai, and Zhenlou Chen

Cite This: *Environ. Sci. Technol.* 2021, 55, 7287−7298

Read Online

ACCESS | Metrics & More | Article Recommendations | Supporting Information

**ABSTRACT:** Rivers and streams contribute significant quantities of methane ($CH_4$) to the atmosphere. However, there is a lack of $CH_4$ flux and ebullitive (bubble) emission data from urban rivers, which might lead to large underestimations of global aquatic $CH_4$ emissions. Here, we conducted high-frequency surveys using the boundary layer model (BLM) supplemented with floating chambers (FCs) and bubble traps to investigate the seasonal and diurnal variability in $CH_4$ emissions in a eutrophic urban river and to evaluate whether the contribution of bubbles is important. We found that ebullition contributed nearly 99% of $CH_4$ emissions and varied on hourly to seasonal time scales, ranging from 0.83 to 230 mmol m$^{-2}$ d$^{-1}$, although diffusive emissions and $CH_4$



concentrations in bubbles did not exhibit temporal variability. Ebullitive $CH_4$ emissions presented high temperature sensitivity ($r = 0.6$ and $p < 0.01$) in this urban river, and eutrophication might have triggered this high temperature sensitivity. The ebullitive $CH_4$ flux is more likely to be underestimated at low temperatures because capturing the bubble flux is more difficult, given the low frequency of ebullition events. This study suggests that future ebullition measurements on longer time scales are needed to accurately quantify the $CH_4$ budgets of eutrophic urban rivers.

**KEYWORDS:** $CH_4$ emissions, bubbles, urban river, temporal variability, warming effect
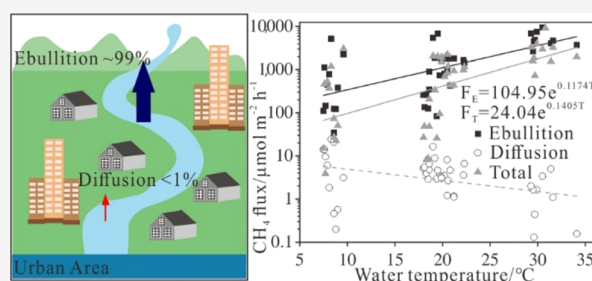
## 1. INTRODUCTION

Inland freshwater ecosystems (particularly ponds, lakes, rivers, and reservoirs) play significant roles in the global carbon cycle[1−4] and inventories of greenhouse gases (GHGs).[5−7] It has been suggested that methanogenesis accounts for as much as 10−50% of the overall carbon mineralization in freshwater environments,[8] resulting in a large amount of methane ($CH_4$) outgassing to the atmosphere.[9,10] Streams and rivers are considered significant sources of $CH_4$, with estimated emissions of 1.5−26.8 Tg yr$^{-1}$,[11−14] corresponding to 1−18% of global nonanthropogenic emissions and 0.3−5.3% of total $CH_4$ emissions.[15,16] Eutrophic fluvial systems, especially those located in urban areas and impacted by human activities, emit considerable $CH_4$[17−22] and are expected to have a greater contribution to aquatic $CH_4$ emissions in the future with the continuous development of urbanization.[23] However, critical uncertainties still exist in terms of the magnitude and regulation of $CH_4$ emissions from eutrophic fluvial systems[24,25] due to the complexities of the processes underlying aquatic $CH_4$ emissions[26] and the lack of available measured data in urban rivers and streams.[11] More attention on fluvial $CH_4$ emission measurements and better recognition of inland waters as $CH_4$ sources can not only substantially affect global GHG inventories but also broaden the understanding of ecological carbon cycle functioning in rivers and streams.

There are three flux pathways for the emission of $CH_4$ from freshwater: the plant-mediated flux (not discussed in this study), molecular diffusion, and bubble transmission (ebullition).[11] Ebullition prevents $CH_4$ from being oxidized in the water column and emits it to the atmosphere directly.[26−29] Previous studies have reported that the ebullition of $CH_4$ accounts for a large proportion (up to 90%) of the total $CH_4$ emissions.[12,30−33] Nevertheless, few studies have simultaneously investigated $CH_4$ diffusion and ebullition in urban rivers, and the contribution of ebullitive $CH_4$ emissions from urban rivers to the global carbon budget is likely underestimated.[22] To understand the magnitude of aquatic $CH_4$ emissions, it is necessary to integrate these pathways and understand the spatiotemporal variations in their relative contributions across aquatic systems.[26]

Aquatic $CH_4$ emissions are driven by $CH_4$ production, which is believed to occur mostly in shallow sediment pore waters stimulated by carbon-rich substrates and anoxic

conditions.[24,34,35] In addition, methanogenesis is highly sensitive to temperature, and ebullitive $CH_4$ fluxes may be more sensitive to changes in temperature than diffusive fluxes.[36,37] A synergistic interaction between the influence of increasing temperature and nutrient enrichment has been observed in many freshwater systems, which leads to a disproportional increase in aquatic $CH_4$ emissions.[38−41] In the case of urban areas, streams and rivers, which generally receive effluent discharges that are rich in organic matter (OM) and nutrients, contribute greatly to $CH_4$ production.[16,23] In addition, the urban heat island effect causes higher temperatures in urban areas than in surrounding areas.[42] Thus, considering the trend of global mean temperature and the increasing eutrophication of rivers by human activities,[43] a more mechanistic understanding of the $CH_4$ emissions in urban rivers is required if we hope to predict the global aquatic $CH_4$ inventories and to achieve a more integrated understanding of the current and future role of fluvial systems in regional and global C cycles.

In addition, $CH_4$ ebullition is most likely underestimated due to the episodic characteristics and high spatiotemporal heterogeneity of bubble events. Previous studies, however, mostly concentrated on spatial (horizontal and vertical) differences in ebullitive $CH_4$ emissions,[24,31,32] and few have studied the temporal variability, especially with short-term measurements. Random ebullition "hotspots" are easily missed by the usual short-term (<24 h) and low-frequency (>1 h interval) measurements,[30,41] resulting in the underestimation of total $CH_4$ emissions. Accordingly, higher sampling frequencies and longer sampling periods are required to precisely describe the magnitude and regulation of ebullitive emissions from rivers.[38,44,45]

In this study, we selected a mesotrophic river located in Shanghai, China, which has undergone intense urbanization over the past decades. We used three different methods, the boundary layer model (BLM), floating chambers (FCs), and bubble traps, to conduct high temporal resolution continuous measurements of diffusive and ebullitive $CH_4$ emissions over a year. The BLM flux measurement is convenient and easy to operate, but it omits the potentially important fluxes of ebullition events.[25,46,47] The FC method and bubble traps are advantageous since they capture ebullition,[12,30,48] but they are laborious and can cause disturbance of the air−water interface in running water. Each approach has pros and cons, and it is necessary to choose or integrate multiple methods to minimize the estimation error due to the sampling method.[49]

The objectives of this study are to (1) document the important role of ebullition events on $CH_4$ transport from an urban river and explore what determines the release of bubbles; (2) compare the differences among the magnitudes of $CH_4$ fluxes measured by three different approaches; and (3) explore the temporal variation in $CH_4$ fluxes in river systems to minimize the error in estimating regional and global $CH_4$ budgets.

## 2. MATERIALS AND METHODS

**2.1. Study Area.** Shanghai, located in eastern China, is the economic and financial center of the Yangtze Delta. There are more than 3000 rivers in Shanghai, and Suzhou Creek is one of the major rivers in this area. It is the tributary of the Wusong River and is approximately 53.1 km long from west to east and 40−50 m wide on average. The urban reach of Suzhou Creek has suffered severe water pollution since the 19th century due

to intense urbanization, accompanied by the discharge of large amounts of industrial wastewater and domestic sewage directly into the river. After more than 20 years of pollution treatment, the water quality in Suzhou Creek has been greatly improved and has remained at level V (Standard for Environmental Quality of Surface Water of the People's Republic of China, 2002) since 2011. The average river discharge is only 10 $m^3$/s, with a slow annual water velocity of approximately 0.1 m/s. The climate of the study area is characterized by hot summers and warm winters, and the annual average temperature is 17.5 °C. The average annual precipitation is 1510 mm, with 70% of the total precipitation occurring from May to September.

In this study, we selected a sampling point located in the urban reach of Suzhou Creek that is almost entirely surrounded by residential areas (Figure S1). All the sampling work was carried from a pier (Figure S1) that extends into the river (approximately 10 m from the bank). The river width and water depth at sampling sites are ~40 and ~2 m, respectively. According to our measurements, the annual mean ammonia ($NH_4^+$), nitrate ($NO_3^-$), and chlorophyll a (Chla) concentrations in the water column are 1.54 mg/L, 1.91 mg/L, and 47.4 $\mu$g/L, respectively (Table S1). The surface sediment organic carbon (OC) content is approximately 2% by mass, and the dissolved organic carbon (DOC) concentration is approximately 17 mg/L, as measured in July 2018.

**2.2. Rate of Bubble Release.** We deployed opaque inverted funnel-style bubble traps to determine the volume of bubbles emitted from the sediments. The sampling equipment was deployed from a pier that extends into the middle of the river. All sampling in this study, including dissolved gas and FC measurements, was performed on the platform of this pier. We set three adjacent (~5 m) traps to eliminate the spatial differences and highlight the temporal variations in the ebullition events. The sampling was conducted during different seasons: autumn (November 2018), winter (January 2019), spring (April 2019), and summer (July 2019). Each sample was taken continuously for 36 h, from 9:00 to 15:00 on the next day.

The bubble trap is similar to a large funnel with a bottom surface area of ~0.79 $m^2$, and the stem was replaced by a syringe with a three-way stopcock (Figure S2). The narrow neck of the trap could limit the potential diffusion of $CH_4$ back into the water. Traps were affixed to steel poles on the pier and installed almost completely submerged. Traps were filled completely with water and contained no headspace at the start of each sampling event. The ebullition rates were calculated by recording the volume of gas and sampling time. The cumulative gas volume was recorded by the scale on the syringe. The sampling frequency was determined by the rate of bubbles trapped in the syringe, and measurements were generally recorded once every 5 min. Higher frequency (<5 min) measurements were required when the ebullition rate was so fast that the gas filled the whole syringe. In contrast, when the ebullition rate was too slow for gas to accumulate in the syringe (generally occurring at night), gas was collected until the gas volume could be recorded. By dividing the cumulative volume of gas by the time interval, we calculated the ebullition rates over the corresponding period. We assumed that the rate within each time period was constant, and then, we obtained the change in minute-scale ebullition rates.

**2.3. Measurements of $CH_4$ Emissions.** Three measurement methods, bubble traps, the BLM, and FCs, were used to estimate ebullitive, diffusive, and total $CH_4$ fluxes, respectively.

The ebullition rates and ebullitive $CH_4$ emissions that appear below were all measured by the bubble trap approach.

*2.3.1. Ebullitive $CH_4$ Emissions.* We collected bubbles during different time periods (morning/noon/evening/midnight) and from different traps in every sampling season to examine the $CH_4$ concentration in the bubbles. Collected bubbles were transferred into prevacuumed gas bags, taken back to the lab, and analyzed by an Agilent HP7890 gas chromatograph equipped with a flame ionization detector (FID).

The ebullitive $CH_4$ fluxes were calculated using eq 1

$$\text{ebullitive } CH_4 \text{ flux} = C_B \times V_B \tag{1}$$

where $C_B$ is the $CH_4$ concentration in the bubbles ($\mu$mol L$^{-1}$) and $V_B$ is the bubble rate (mL m$^{-2}$ d$^{-1}$).

*2.3.2. Diffusive $CH_4$ Emissions.* We sampled surface water for dissolved gas analysis, and the measurements were carried out every 3 h, from 9:00 to 15:00 on the next day, with 11 sampling events in total. Samples were taken in 138 mL polymethyl methacrylate glass tubes with no headspace, capped with butyl rubber stoppers, and field preserved with saturated mercuric chloride to avoid microbial activities. Samples were transported to the laboratory and analyzed within 48 h.

A headspace equilibration technique was created by injecting 60 mL of ultrapure $N_2$ into the water sample. The tube was left with $\sim$78 mL of the water sample, and then, we shook the tube vigorously for 3 min to let gas diffuse out and $CH_4$ equilibrate between the water–air interface. After the gas in the sampling tube reached balance (setting for approximately 20 min), we obtained gas samples from the top of the tube and analyzed the $CH_4$ concentration as described above.

Diffusive $CH_4$ emissions were calculated using the BLM method[50]

$$\text{diffusive } CH_4 \text{ flux} = k(C_w - C_{eq}) \tag{2}$$

where $k$ is the piston velocity (m h$^{-1}$); $C_w$ is the measured $CH_4$ concentration in the water calculated with the Bunsen coefficient ($\mu$mol L$^{-1}$); and $C_{eq}$ is the water saturation of the $CH_4$ concentration ($\mu$mol L$^{-1}$). For this study, the gas transfer velocity was calculated using eq 3[51]

$$k = 1.91e^{0.35U_{10}}(S_C/600)^{-1/2} \tag{3}$$

where $S_C$ is the Schmidt number for $CH_4$ corrected by the in situ water temperature and $U_{10}$ is the long-term wind speed at a height of 10 m above the river. Because the wind speed fluctuates frequently in a short period of time, we obtained hourly average 10 m wind speeds at the sampling site from the website of the Shanghai Meteorological Bureau (http://www.weather.com.cn) for the whole study period and calculated the monthly average wind speed for a conservative $CH_4$ flux calculation.

*2.3.3. Total $CH_4$ Emissions.* Floating chambers with a 0.6 m diameter and a total volume of $\sim$28 L were used to measure total $CH_4$ emissions (Figure S2). Each chamber was covered with aluminum foil to reduce sun heating, and a rubber tube was connected to the inside of the chamber and used to collect the air sample. Each chamber was deployed near a bubble trap. To measure the $CH_4$ flux, gas samples were withdrawn from the chamber space with a syringe through a three-way stopcock 10, 20, and 30 min after the chambers were set on the water surface. First, we extracted 60 mL of gas twice to expel the

remaining gas in the rubber tube, and then, 60 mL of gas was extracted for a third time as a sample. The gas samples for $CH_4$ were stored and analyzed similar to the bubble samples. We carried out chamber measurements every time we sampled headspace gas for diffusive flux calculation. The total $CH_4$ fluxes were calculated using the following equation

$$\text{total } CH_4 \text{ flux} = (\Delta s \times V_c)/(\Delta t \times A) \tag{4}$$

where $\Delta s$ ($\mu$mol L$^{-1}$) is the difference in the gas concentration in the chamber over time; $V_c$ (L) is the volume of the chamber; $\Delta t$ (h) is the sampling time; and $A$ (m$^2$) is the surface area of the chamber.

**2.4. Other Measurements.** In each sampling event, we measured the water temperature, dissolved oxygen (DO) concentration, and pH using a multiparameter probe (HACH, Danaher, Loveland, CO, USA). Water samples were taken at 0.2 m below the surface in each field campaign. These samples were used to measure the concentrations of Chla, $NH_4^+$, and $NO_3^-$. Chla was determined spectrophotometrically on Whatman GF/F-filtered samples following sonication and pigment extraction with 90% acetone. Dissolved $NH_4^+$ and $NO_3^-$ were analyzed using Nessler's reagent spectrophotometry and zinc cadmium reduction, respectively. The surface sediment OC content was analyzed via potassium dichromate oxidation spectrophotometry.

**2.5. Ecosystem-Level $Q_{10}$ and Activation Energy ($E_a$).** The $Q_{10}$ value is often used to represent the proportional changes in a process per 10 °C temperature change. Due to the combined effects of multiple factors on $CH_4$ emissions, we used the ecosystem-level $Q_{10}$, not the physiological $Q_{10}$, to evaluate the temperature dependency of $CH_4$ emissions. We calculated the ecosystem-level $Q_{10}$ using the equation $Q_{10} = 10^{10b}$, where $b$ is the slope of the linear regression between a data set of water temperatures and log-transformed $CH_4$ emissions.[26]

Additionally, the sensitivity of ebullitive $CH_4$ emissions to temperature was also assessed through the apparent activation energy ($E_a$), which was obtained from the slope of the Arrhenius equation

$$\ln(F_T) = \ln(A) - \left(\frac{E_a}{R} \times \frac{1}{T}\right) \tag{5}$$

where $\ln(F_T)$ ($\mu$mol m$^{-2}$ h$^{-1}$) is the log-transformed bubble flux at the absolute temperature $T$ (K); $A$ is the Arrhenius constant, which is experimentally determined; and $R$ is the universal gas constant (8.314 J mol$^{-1}$ K$^{-1}$).

**2.6. Analysis.** *2.6.1. Calculation of the Total $CH_4$ Emissions.* In addition to obtaining the total $CH_4$ emissions via the FC approach, we can also calculate the total $CH_4$ emissions by adding the diffusive and ebullitive $CH_4$ emissions. Since the diffusive emissions comprise many discrete values, the ebullitive emissions were averaged over the corresponding period first, and then, the diffusive and ebullitive emissions were added together. For instance, we calculated the total $CH_4$ emissions at 9:00 by adding the diffusive emissions at 9:00 with the mean ebullitive emissions in the period of 9:00–10:00. The total emissions obtained by this addition were approximately the same as the emissions obtained by the FC approach.

*2.6.2. Estimating the Representative Measurement Duration by Subsampling.* Our data set consists of ebullitive $CH_4$ emission measurements taken over 36 h in each sampling

season. Subsets of data covering 1–16 h were randomly selected from the total data set (~36 h in total). The mean ebullitive emissions of the subset ($E_{subset}$) were compared with the 90% confidence interval (CI) of the total data set. When $E_{subset}$ was in the range of the CI of the total data set, $E_{subset}$ could represent the values in the whole sampling period. Each subset was tested 1000 times, and we calculated the probability that $E_{subset}$ was within the 90% CI of the total data set for each subset. When this probability reached 80% for a subset, we considered the time of that subset to be the representative measurement duration.

*2.6.3. Statistical Analysis.* All statistical tests were performed using SPSS (Version 23.0, SPSS Inc., Chicago, IL, USA). We examined the seasonal and hourly temporal variability in all $CH_4$ fluxes, and data were log-transformed to a normal distribution before the statistical analysis was performed. Differences among seasons and sampling points were examined using independent sample *t*-tests. Differences in total fluxes calculated based on different sampling times were examined using one-way ANOVA. Linear regression between individual or combined variables and $CH_4$ emissions was conducted and tested for significance. Pearson correlation was used to examine the correlations among independent variables. All statistical tests used a significance level of 5% ($\alpha = 0.05$).

## 3. RESULTS

**3.1. Ebullition Events.** There were significant differences in ebullition rates among seasons, with the exception of no obvious differences between November and January or between November and April (Table S2). The mean ebullition rate over 36 h was the highest in July ($3300 \pm 1400$ mL m$^{-2}$ d$^{-1}$), followed by April ($1100 \pm 450$ mL m$^{-2}$ d$^{-1}$), November ($950 \pm 1600$ mL m$^{-2}$ d$^{-1}$), and January ($570 \pm 910$ mL m$^{-2}$ d$^{-1}$), consistent with the mean temperatures (30.8 °C in July, 20.9 °C in April, 18.8 °C in November, and 8.3 °C in January). The high standard deviations of the mean rates illustrate the stochastic nature of ebullition events. In addition, we compared the ebullition rates from different sampling traps in each sampling season, and the results (Table S3) also suggested that ebullition was a stochastic event.

The ebullition rates showed distinct diurnal changes in all seasons. In November and January, the daily peak occurred during the period from 10:00 to 15:00, followed by a second peak during the period from 21:00 to 1:00 (Figure 1a,b). High ebullition rates occur frequently for long durations in April and July (Figure 1c,d). The coefficients of variation were greater in November and January (174 and 160%, respectively) than in April and July (40 and 43%, respectively).

The frequency distributions of ebullition rates (in 24 h, from 13:00 to 13:00 the next day) in November and January were highly positively skewed, with median values (240 and 160 mL m$^{-2}$ d$^{-1}$, respectively) smaller than the mean values (380 and 600 mL m$^{-2}$ d$^{-1}$, respectively) (Figure 2a,b). The frequency distributions in April and July were less skewed and closer to a normal distribution, with medians (1200 and 3100 mL m$^{-2}$ d$^{-1}$, respectively) close to the means (1200 and 3200 mL m$^{-2}$ d$^{-1}$, respectively) (Figure 2c,d).

To quantify the contribution of ebullition events to $CH_4$ emissions, the concentrations of three GHGs were measured in bubbles at each of the sampling points. Table S4 shows that each collected bubble had a similar proportion of GHGs, and among the three GHGs, $CH_4$ had the highest concentration ($66.3 \pm 4.3\%$ by volume).
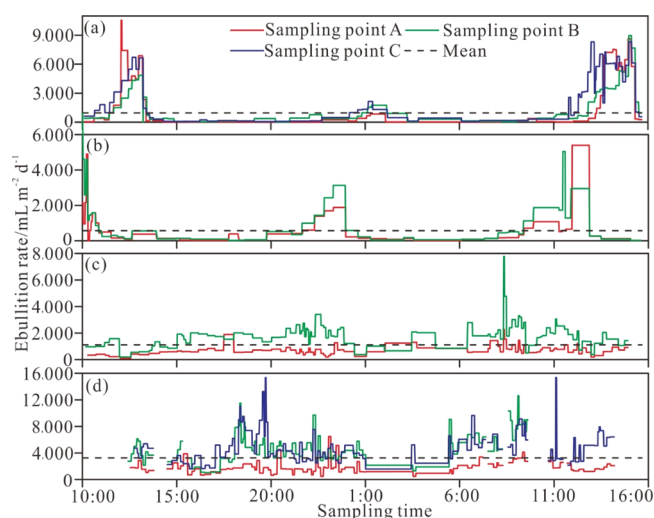


**Figure 1.** Ebullition rates at each sampling point (A, B, and C) in November 2018 (a), January 2019 (b), April 2019 (c), and July 2019 (d). The sampling event in July 2019 was affected by a high frequency of passing ships during the daytime period (9:00–13:00), which resulted in some defaulted values during the daytime.
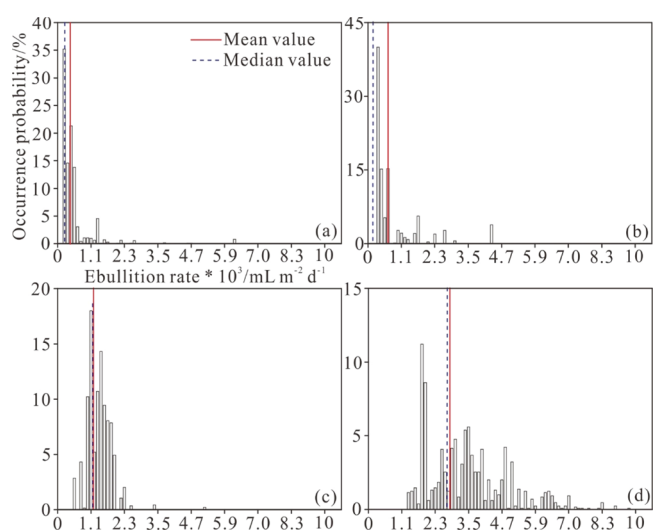


**Figure 2.** Probability distribution of ebullition rates in November 2018 (a), January 2019 (b), April 2019 (c), and July 2019 (d).

**3.2. Comparison of $CH_4$ Fluxes.** The total $CH_4$ flux can be calculated by summing the ebullitive flux and the diffusive flux, and the results show that the ebullition events contributed up to $98 \pm 6.3\%$ of the total flux (Table S5). The chamber $CH_4$ flux was equal to the total $CH_4$ flux because the floating chamber can simultaneously measure both diffusive and ebullitive fluxes. The chamber $CH_4$ fluxes were strongly correlated with ebullitive $CH_4$ fluxes ($r = 0.81$ and $p < 0.05$), and there was no obvious correlation with diffusive $CH_4$ fluxes (Table S6). We calculated the total $CH_4$ flux over different time intervals (10, 20, and 30 min) by the FC approach, and the results show that the fluxes calculated for the first 10 min were significantly higher than those calculated for the two other intervals ($F = 4.236$ and $p = 0.017$). In addition, the chamber fluxes calculated for 20 min and 30 min intervals were consistent with the change in bubble fluxes (Figure 3). However, the total $CH_4$ fluxes measured by the FC method were underestimated compared with the sum of the ebullitive
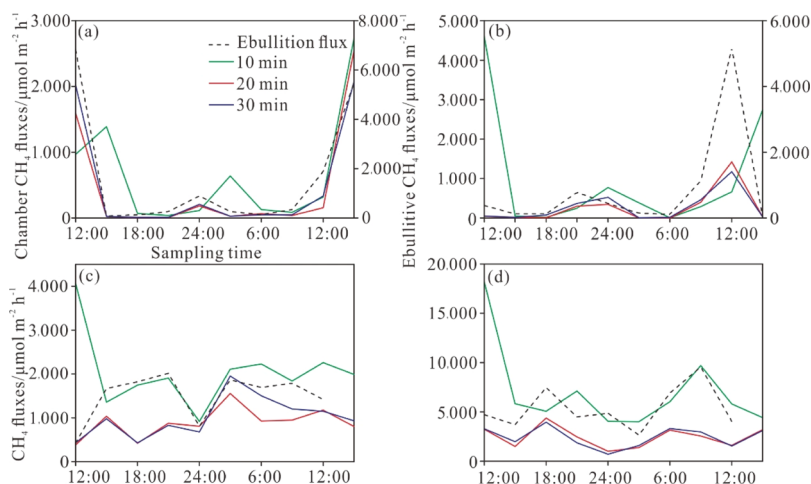
**Figure 3.** Comparison of the chamber fluxes calculated for three-time intervals (10, 20, and 30 min) and the ebullitive fluxes in November 2018 (a), January 2019 (b), April 2019 (c), and July 2019 (d).

and diffusive fluxes. The total $CH_4$ fluxes via the FC method might be underestimated by $61 \pm 27\%$ (20 min interval) and $57 \pm 30\%$ (30 min interval) (Table S5). The following analysis was based on the chamber flux at 30 min time intervals to minimize the sampling biases.

**3.3. Temporal Variability of $CH_4$ Fluxes.** There were obvious seasonal differences in ebullitive $CH_4$ emissions, with the maximum value in July ($4800 \pm 1800$ $\mu$mol m$^{-2}$ h$^{-1}$), followed by April ($1600 \pm 500$ $\mu$mol m$^{-2}$ h$^{-1}$), November ($1400 \pm 2200$ $\mu$mol m$^{-2}$ h$^{-1}$), and January ($800 \pm 1200$ $\mu$mol m$^{-2}$ h$^{-1}$) (Figure 4a). Similar seasonal variations in chamber $CH_4$ fluxes were found, with the highest values in July ($3100 \pm 2300$ $\mu$mol m$^{-2}$ h$^{-1}$), followed by April ($1100 \pm 590$ $\mu$mol m$^{-2}$ h$^{-1}$), January ($530 \pm 910$ $\mu$mol m$^{-2}$ h$^{-1}$), and November ($450 \pm 800$ $\mu$mol m$^{-2}$ h$^{-1}$) (Figure 4c). However, Figure 4b

illustrates the opposite seasonal characteristics: the diffusive $CH_4$ flux reached the peak value in January ($8.63 \pm 8.60$ $\mu$mol m$^{-2}$ h$^{-1}$), followed by November ($5.90 \pm 3.86$ $\mu$mol m$^{-2}$ h$^{-1}$), April ($3.53 \pm 2.22$ $\mu$mol m$^{-2}$ h$^{-1}$), and July ($1.59 \pm 1.55$ $\mu$mol m$^{-2}$ h$^{-1}$).

In this study, diurnal fluctuations in $CH_4$ fluxes were analyzed by successive observation experiments over 36 h in each sampling season. For the diurnal fluctuations in ebullitive emissions, there were similar diurnal changes in November and January and complex variations in April and July (Figure 5a). There were two peak values that occurred in November and January, with the maximum value at noon and the second peak value at midnight, but no significant peak value was observed in April or July. Similar mean ebullitive fluxes between the daytime and the nighttime were found in January ($950 \pm 1300$ and $620 \pm 950$ $\mu$mol m$^{-2}$ h$^{-1}$, respectively), April ($1600 \pm 580$ and $1600 \pm 400$ $\mu$mol m$^{-2}$ h$^{-1}$, respectively), and July ($5000 \pm 1800$ and $4600 \pm 1700$ $\mu$mol m$^{-2}$ h$^{-1}$, respectively) (Figure 5b). There was a significant difference in ebullitive emissions between the daytime ($2100 \pm 2700$ $\mu$mol m$^{-2}$ h$^{-1}$) and the nighttime ($490 \pm 480$ $\mu$mol m$^{-2}$ h$^{-1}$) in November ($t = 2.394$ and $p = 0.028$, Figure 5b).

The diurnal variation in diffusive $CH_4$ fluxes showed only a slight fluctuation in all seasons (Figure 5c). However, there was an obvious difference ($t = 2.253$ and $p = 0.03$) in diffusive fluxes between day and night. The average diffusive fluxes during the daytime ($6.87 \pm 4.62$ in November, $11.0 \pm 9.82$ in January, $4.24 \pm 2.41$ in April, and $1.95 \pm 1.81$ $\mu$mol m$^{-2}$ h$^{-1}$ in July) were larger than those during the nighttime ($4.20 \pm 1.01$ in November, $4.47 \pm 4.15$ in January, $2.27 \pm 1.26$ in April, and $0.96 \pm 0.79$ $\mu$mol m$^{-2}$ h$^{-1}$ in July) (Figure 5d).

As shown in Figure 5e, the highest chamber flux generally occurred during the period of 9:00−12:00. The average $CH_4$ fluxes during the daytime ($660 \pm 950$ in November, $690 \pm 1100$ in January, $1200 \pm 570$ in April, and $3600 \pm 2500$ $\mu$mol m$^{-2}$ h$^{-1}$ in July) were larger than those during the nighttime ($62.5 \pm 96.4$ in November, $243 \pm 246$ in January, $970 \pm 670$ in April, and $2000 \pm 1400$ $\mu$mol m$^{-2}$ h$^{-1}$ in July) (Figure 5f).

**3.4. Temperature Effect and Ecosystem-Level $Q_{10}$.** We analyzed the correlation between the $CH_4$ fluxes and water temperature and found that both ebullitive fluxes and chamber fluxes were positively correlated with temperature ($r = 0.6$ and $p < 0.05$ and $r = 0.54$ and $p < 0.05$, respectively), but the
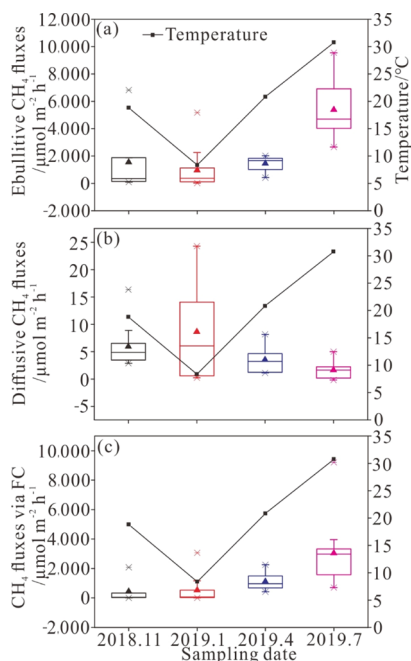


**Figure 4.** Seasonal variations in ebullitive $CH_4$ fluxes (a), diffusive $CH_4$ fluxes (b), and $CH_4$ fluxes via the FC method (c) compared with temperature changes.
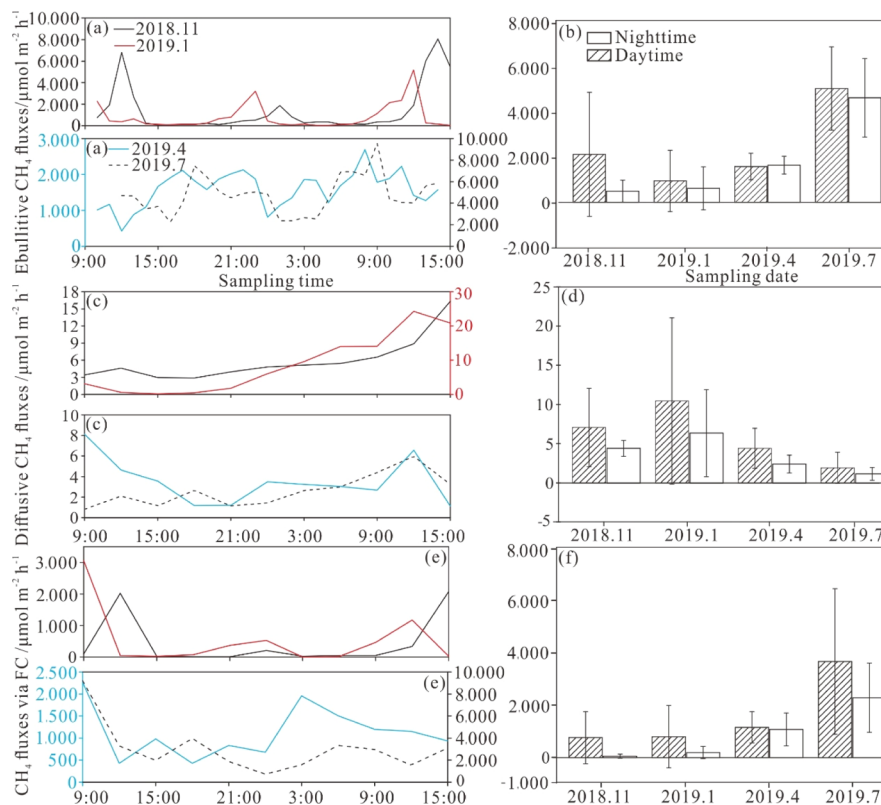
**Figure 5.** Diurnal variations in ebullitive $CH_4$ fluxes (a), diffusive $CH_4$ fluxes (c), and $CH_4$ fluxes via FC (e) in different seasons and comparisons of daytime (7:00−17:00) and nighttime (18:00−6:00 on the next day) averages with ebullitive $CH_4$ fluxes (b), diffusive $CH_4$ fluxes (d), and $CH_4$ fluxes via FC (f) in different seasons. Figures with a large difference in maximum values have two vertical coordinates, and the curve values correspond to the same-colored vertical coordinate.
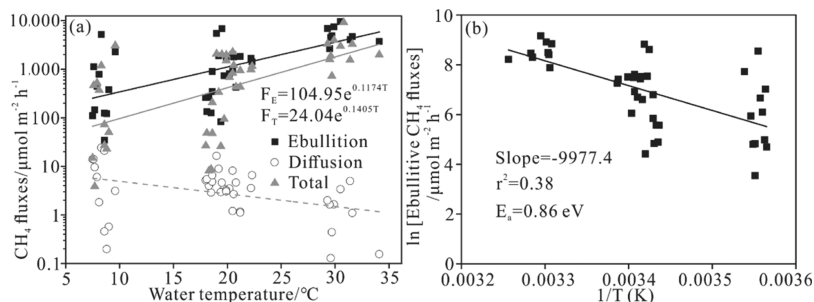


**Figure 6.** (a) Linear regressions of the ebullitive flux (black squares), diffusive flux (gray triangles), and total flux (the sum of ebullitive and diffusive fluxes) (circles) versus water temperature. The vertical coordinate of flux is replaced by the exponential coordinate and represents exponential fit. The exponential equation represents an exponential relationship between ebullitive ($F_E$), total ($F_T$) flux, and temperature, respectively. The linear equations are shown in Table 1. (b) Arrhenius-style plot with ln(ebullitive $CH_4$ flux) vs the inverse water temperature in K.

**Table 1. Linear Regression Equations**

| $CH_4$ emissions | predictor | equation | N | p value | $r^2$ |
|---|---|---|---|---|---|
| diffusion | $T_w$ | $\log_{10}(CH_4\ \text{diffusion}) = -0.025 \times T_w + 0.936$ | 42 | 0.014 | 0.14 |
| | $T_w$ + DO | $\log_{10}(CH_4\ \text{diffusion}) = -0.021 \times T_w + 0.76 \times \log_{10}(DO) + 0.455$ | 41 | 0.005 | 0.24 |
| ebullition | $T_w$ | $\log_{10}(CH_4\ \text{ebullition}) = 0.051 \times T_w + 2.021$ | 40 | <0.001 | 0.40 |
| | $T_w$ + DO | $\log_{10}(CH_4\ \text{ebullition}) = 0.047 \times T_w - 0.66 \times \log_{10}(DO) + 2.452$ | 40 | <0.001 | 0.47 |
| chamber fluxes | $T_w$ | $\log_{10}(\text{chamber}\ CH_4\ \text{fluxes}) = 0.061 \times T_w + 1.381$ | 42 | <0.001 | 0.32 |
| | $T_w$ + DO | $\log_{10}(\text{chamber}\ CH_4\ \text{fluxes}) = 0.055 \times T_w - 0.875 \times \log_{10}(DO) + 1.963$ | 41 | <0.001 | 0.35 |

diffusive fluxes were negatively correlated with temperature ($r$ = −0.48 and $p$ < 0.05) (Table S6). Based on the strong temperature dependency of $CH_4$ emissions, the ecosystem-level $Q_{10}$ and $E_a$ for ebullition were 3.25 and 0.86, respectively, and the $Q_{10}$ value of diffusive $CH_4$ emissions was 0.56 (Table

S7). The linear regression between water temperature and $CH_4$ emissions further supported the effect of warming on diffusive fluxes and especially on ebullitive fluxes (Figure 6), explaining 14 and 40% of the variability, respectively (Table 1). Multiple regression models with water temperature and DO explained

higher proportions of the variability in both diffusive and ebullitive $CH_4$ emissions (24 and 47%, respectively) (Table 1).

## 4. DISCUSSION

**4.1. Contribution of Ebullition to Total $CH_4$ Emissions.** With the addition of the data in this study, bubble releases have now been reported among different seasons, documenting the frequent occurrence of ebullition events in urban rivers. Compared with the limited $CH_4$ ebullition studies of freshwater systems, we found that the ebullition rates in the studied urban river were much higher than those in other rivers or lakes (from 2 to 200 mL m$^{-2}$ d$^{-1}$[24,26,32,45]). Although the ebullition rates in streams given by Baulch et al. (2011)[24] and Crawford et al. (2014)[32] were observed to be as high as >2000 mL m$^{-2}$ d$^{-1}$, these rates are still lower than the mean ebullition rate in the studied river during summer (>3000 mL m$^{-2}$ d$^{-1}$). Our ebullition rates are comparable to those from another megacity in China (Beijing: 77 ± 62 mL m$^{-2}$ h$^{-1}$), which further confirms that ebullition plays an important role in $CH_4$ transport in shallow aquatic environments.[11,22,52]

In addition, the $CH_4$ concentration in bubbles (% $CH_4$) is another important factor because it directly impacts ebullitive $CH_4$ emissions.[26] Several studies have reported a wide range of % $CH_4$ (<1 to >90%, Table S8), resulting in large variability in ebullitive $CH_4$ emissions.[26,45] $CH_4$ concentrations are regulated by both production and consumption processes. High sediment OC contents, low DO concentrations, and shallow water depths promote $CH_4$ production and reduce $CH_4$ dissolution and oxidation in the water column, which increase % $CH_4$.[22] In addition, temporal variations in $CH_4$ production and transport may affect the relative concentration of $CH_4$ in bubbles.[24] A large increase in %$CH_4$ was observed during summer in a subarctic lake.[45] However, our study found a similar $CH_4$ content (65%) in the collected bubbles among different seasons, which is consistent with the results of Crawford et al. (2014).[32] We hypothesize that the high OC content and high nutrient levels (Table S1) with little substrate limitation resulted in the high % $CH_4$ and the lack of seasonal variation in % $CH_4$ in this study.[53] The temperature effect on % $CH_4$ might be limited in shallow and OC-rich sediments.

Combining ebullition rates and % $CH_4$ in bubbles, our research indicates that ebullition might be a largely underestimated pathway of $CH_4$ emissions in rivers and streams. Bubble fluxes in the studied river accounted for up to 99% of the total $CH_4$ fluxes, and the total $CH_4$ fluxes in the studied river were higher than those in other rivers and were comparable to those in some lakes and reservoirs (see Table S8). Some agricultural streams and rivers have developed high ebullitive emissions because of OM-rich sediments, which came from either autochthonous or allochthonous OM inputs. A large amount of OM has been buried in the sampling reach of Suzhou Creek, which used to be the densest industrial area in central Shanghai city, due to the large input of pollutants and sewage. We found that agricultural and urban rivers (~11.7 mmol m$^{-2}$ d$^{-1}$[19,21,22,24,31,40,54,55]) have a greater potential for $CH_4$ emissions than pristine rivers (~1.63 mmol m$^{-2}$ d$^{-1}$[12,19,32,56−59]) (Figure S3). These results are consistent with higher concentrations of OM and other nutrients ($NH_4^+$, $NO_3^+$, and Chla) in urban river water columns and sediments. In addition, the OM composition and quality also affect $CH_4$ production.[43] Urban rivers receive OM from large inputs of domestic sewage, which increases the amounts of anthropogenic fulvic acid-like and protein-like

dissolved organic matter (DOM)[60] and is more easily degraded than OM from agricultural waste. The high nutrient levels in the studied urban river also stimulate phytoplankton or macrophyte growth and thus provide more inputs of autotrophic OC, which promotes methanogenesis and bubble release.[61,62] Thus, our results indicate a higher proportion of ebullition in the studied river than in other agricultural-dominated freshwaters (see Table S8). In addition, the increase in $CH_4$ production by labile OM far exceeds the potential dissolution of $CH_4$, resulting in enhanced $CH_4$ ebullition.[43] Given that urban rivers might receive high nutrient inputs from human activities, further studies of ebullitive $CH_4$ fluxes cannot be excluded when upscaling aquatic $CH_4$ emissions, and future attention should be focused on the linkage between OM composition and ebullitive $CH_4$ emissions.

**4.2. Temperature Effect.** Aquatic $CH_4$ emissions have temporal variability as a consequence of both biotic and abiotic parameters, and these external forcing act on different time scales, resulting in both short-term and long-term variabilities in gas emissions.[63] Our results show that both diurnal and seasonal variations in bubble fluxes had significant correlations with water temperature, which indicates that the temperature within the shallow sediment responds quickly to water temperature changes.[45] The temperature-ebullition exponential relationship (Figure 6a) indicated that climate warming will increase $CH_4$ ebullition by 12.5% per 1 °C warming, which is within the range of other freshwater ecosystems (6−20%).[44] The higher ecosystem-level $Q_{10}$ values for ebullition than for diffusion also demonstrated the high temperature dependency of bubble emissions. Similar results have been reported in which $Q_{10}$ values for ebullition were higher than those for diffusion.[26,64] Although the $Q_{10}$ value for ebullition in our study was lower than the $Q_{10}$ values in other ponds and lakes (Table S7), the overall higher ebullitive $CH_4$ emissions from our studied river still grossly exceeded $CH_4$ emissions from other aquatic systems. For example, if a 10 °C increase in water temperature was to increase bubble emissions from our studied river from a mean value of 53−170 mmol m$^{-2}$ d$^{-1}$ ($Q_{10}$: 3.25), the resulting bubble emissions from northern ponds would increase from 4.6 to 60 mmol m$^{-2}$ d$^{-1}$ ($Q_{10}$: 13).[26]

The significant positive relationship between temperature and bubble fluxes in this study might be a result of the synergistic interaction between warming and eutrophication. Several disproportional increases in ebullitive $CH_4$ emissions with temperature have been observed in freshwater systems, and the results have been attributed to combined effects.[38−40,44] This synergy is more likely to occur in OC-rich sediments because the substrate limitation is alleviated, allowing $CH_4$ production to be temperature regulated and more $CH_4$ emissions to be released as bubbles.[26,61,65] Due to the tendency of eutrophic systems to accumulate more OC,[66−68] higher nutrient enrichment in water bodies exacerbates the effect of climate warming on $CH_4$ emissions. In addition, the increased hypoxia in water columns caused by eutrophication may also favor methanogenesis and result in a decrease in aerobic $CH_4$ oxidation, ultimately increasing $CH_4$ emissions.[69] This is consistent with the linear regression results for ebullitive $CH_4$ emissions in this study (Table 1), demonstrating the negative effect of DO on ebullitive $CH_4$ emissions. Considering that the productivity of inland waters is projected to increase over the next century due to climate change and human population growth,[70] a disproportionate

increase in aquatic $CH_4$ emissions may concomitantly occur due to their synergistic effects.

### 4.3. Estimation Biases among Three Measurement Methods.

We reported simultaneous diffusive and ebullitive $CH_4$ emissions and demonstrated biases among different measurement methods. We used the BLM approach to estimate diffusive $CH_4$ emissions and found that the overall diffusive $CH_4$ fluxes fell within the range of reported values from freshwaters, but the proportion of diffusive flux to total flux (∼1%) was lower than that documented in previous studies due to the large contribution of ebullition events in the studied river (Table S8). In addition, the seasonal variation in the diffusive flux, which reached its highest values in winter and lowest values in summer, contrasted with that in the bubble flux, indicating that the proportion of dissolution from bubbles is negligible in summer, although more $CH_4$ was produced in the sediment in summer than in winter.[49] The higher water temperature during summer decreases $CH_4$ solubility and DO concentration in the water column, which promotes more $CH_4$ ebullition rather than oxidation or dissolution in the water column.[33,71] In addition, the diffusive $CH_4$ flux was slightly higher during the daytime than during the nighttime (Figure 5b), and the reasons for this can be twofold. On the one hand, high temperatures during the daytime could stimulate the production of $CH_4$ in the sediment.[72] On the other hand, sunshine may suppress $CH_4$ oxidation, resulting in a larger diffusive $CH_4$ flux in the daytime.[49] Other studies of diel diffusive $CH_4$ emissions also suggested that diffusion would increase linearly when the weather was sunny and the air temperature was higher than the water temperature.[36]

Except for direct ebullition measurements from bubble traps, several studies have obtained the ebullitive flux by calculating the difference between the total $CH_4$ flux measured by the FC method and the diffusive $CH_4$ flux.[12,30,73] However, our results showed that the ebullitive fluxes were ∼60% higher than the total fluxes measured by the FC method, and the biases measured in seasons with higher ebullition rates (July and April) were larger than those in January and October (see Table S5). We suggest that the stochastic nature of ebullition events caused the difference in these two measurements, even though we deployed the FC near the bubble trap. Stochastic ebullition events could explain the fluctuations in $CH_4$ emissions from FC measurements during the study period as well. The difference in $CH_4$ emissions calculated for different time intervals (10/20/30 min) might be due to higher frequency of ebullition event in the first 10 min interval.

The high-resolution monitoring also highlighted the variability in ebullitive $CH_4$ emissions and the total $CH_4$ flux over daily cycles. Ebullitive $CH_4$ emissions and the total $CH_4$ flux varied by 1–2 orders of magnitude over 36 h periods in October and January, which were larger than the corresponding variations in April and July. This result demonstrates that larger episodic ebullition events occurred frequently with higher temperatures at both daytime and nighttime. There were second peak values at night in all sampling seasons, and this result may be related to the thermal convection effect during the nighttime cooling of the surface water.[74] When the water temperature is higher than the air temperature, the diffusive $CH_4$ emissions increase slowly, and the $CH_4$ ebullition increases substantially.[36] Due to the small increase in $CH_4$ ebullition at night, there was no significant difference in ebullitive $CH_4$ emissions between daytime and nighttime in January, April, or July. A similar result was found in Beijing

inland waters, with no significant diurnal variation in ebullition rates.[22]

In this study, we found that the median value of ebullitive flux was closer to the mean value in the warmer season, indicating a lower probability of underestimating the mean flux at higher temperatures. In contrast, the mean flux was more likely to be underestimated at low temperatures. This is because high temperatures are beneficial for the occurrence of a high frequency of ebullition events, and bubbles can be captured more easily within a short measurement duration. The larger underestimation of $CH_4$ emissions by FCs in November and January compared with the values in the same time interval in April and July (Table S5) also confirmed this conjecture. It has been suggested that the period of representative measurement was mostly determined by the temporal gap between ebullition hotspots ("bubbling episodes"), not the ebullition rate itself.[63] We simulated different continuous measurement durations in four sampling seasons to determine the period of representative measurement. We found that three of the four sampling seasons (January, April, and July) had high probabilities (>80%) of achieving relatively accurate (within the 90% CI of the mean emissions of the total sampling time) mean ebullitive $CH_4$ emissions using measurements from a randomly selected 11−12 h period (Figure S4). Since the ebullitive emissions fluctuated the most in November, the likelihood of ignoring some "bubbling episodes" during randomly chosen periods was larger. Hence, a longer sampling duration is needed when bubbling episodes are less frequent.

### 4.4. Implications for Estimates of the Global $CH_4$ Budget.

Recognizing the considerable uncertainty in extrapolating the $CH_4$ flux from only one sampling site to the entire river system, our goal in this study is not to make a rough estimate of the total $CH_4$ flux. Instead, we aim to highlight several major problems in fluvial $CH_4$ research and their implications for future global fluvial/freshwater $CH_4$ emissions based on the characteristics of $CH_4$ emissions in urban rivers.

Our research indicates that ebullition might be a largely underestimated pathway of $CH_4$ emissions in rivers and streams. The large contribution of ebullition events suggests that ebullitive $CH_4$ fluxes cannot be excluded when upscaling $CH_4$ fluxes. Although some studies have made great efforts to determine the global $CH_4$ budget of rivers and streams, for example, updating the global estimate from 1.5 Tg $CH_4$ $yr^{-1}$ to 26.8 Tg $CH_4$ $yr^{-1}$ by integrating more $CH_4$ fluxes,[11,14] there are still several uncertainties due to gaps in the data.

The first gap is the small amount of data that exist, including data on diffusive fluxes and particularly the scarcity of studies on the influence of ebullition on $CH_4$ dynamics. Even though ebullition events exhibit random characteristics with high temporal and spatial variability, their contribution to atmospheric $CH_4$ should not be underestimated.[75] In addition, the global distribution of existing data is uneven, with heavy representation from Europe but a remarkable scarcity in vast continental areas such as Asia.[14] This study confirms the great contribution (up to 99%) of $CH_4$ ebullition from urban rivers to the aquatic $CH_4$ budget and provides measured data support for global estimates. It is necessary to conduct more investigations on $CH_4$ ebullition from urban areas in the future.

The second gap might be caused by the biases among different measuring approaches. First, data measured via the BLM method would strongly underestimate the $CH_4$ fluxes of freshwater systems where ebullition dominates the emission

pathway.[48] Second, after comparing the differences in the bubble flux measured by the FC method and bubble traps, we suggest that the FC method is not as effective as bubble traps for instantaneously capturing ebullition events, resulting in underestimated ebullitive emissions via the FC method. Our results suggest that bubble traps are more suitable for ebullition measurement in high-frequency bubble areas. In addition, the duration of the sampling time affects the ebullitive flux with either method. The underestimation of ebullitive $CH_4$ emissions is largely attributed to the monitoring duration, which easily misses bubble episodes, especially in areas or seasons with a low frequency of ebullition events. Our results suggest that ebullition measurements over a period of 11−12 h during a high-frequency ebullition event period are enough to represent the daily rate. However, ebullitive $CH_4$ emission determinations at low temperatures require longer measurement durations to capture potential ebullition events to prevent significant underestimation of $CH_4$ emissions. These findings have potential implications for future estimates of global fluvial $CH_4$ emissions.

Finally, notably, temperature plays an important role in controlling the ebullition events in the studied river. More importantly, the effect of warming on $CH_4$ emissions, especially ebullitive $CH_4$ emissions, might be grossly exacerbated by an increase in overall system productivity, which is projected to occur due to human population growth and climate changes.[23] Combined with the paucity of work on how the $CH_4$ flux is affected by nutrient enrichment, there are many more uncertainties in quantifying and understanding the $CH_4$ balance of fluvial systems in the future since global climate change and urbanization would strongly change the ecologies of rivers and streams.[14]

## ■ ASSOCIATED CONTENT

### Ⓢ Supporting Information

The Supporting Information is available free of charge at https://pubs.acs.org/doi/10.1021/acs.est.1c00114.

Location of the sampling site and sampling points on the pier; schematic diagram of the floating chamber and bubble trap; diagram of $CH_4$ fluxes collected from previous studies; diagram of success probability trends with increasing subset measurement durations; water chemistry in the studied river; differences in ebullition rates; concentration of different GHGs in the bubbles; comparison of bubble flux, diffusion flux, and total flux via the FC method; correlations among different $CH_4$ fluxes, temperature, and DO; comparison with $Q_{10}$ and $E_a$ from other rivers, lakes, and ponds; and comparison with $CH_4$ fluxes from other rivers, lakes, and reservoirs (PDF)

## ■ AUTHOR INFORMATION

### Corresponding Author

**Dongqi Wang** − *Key Laboratory of Geographic Information Science (Ministry of Education), School of Geographical Sciences, East China Normal University, 200241 Shanghai, China; Yangtze Delta Estuarine Wetland Ecosystem Observation and Research Station, Ministry of Education & Shanghai Science and Technology Committee, East China Normal University, 200241 Shanghai, China*; Phone: +86-21-54341201; Email: dqwang@geo.ecnu.edu.cn

### Authors

**Shu Chen** − *Key Laboratory of Geographic Information Science (Ministry of Education), School of Geographical Sciences, East China Normal University, 200241 Shanghai, China;* ⓞ orcid.org/0000-0001-9656-5249

**Yan Ding** − *Key Laboratory of Geographic Information Science (Ministry of Education), School of Geographical Sciences, East China Normal University, 200241 Shanghai, China*

**Zhongjie Yu** − *Department of Natural Resources and Environmental Sciences, University of Illinois Urbana-Champaign, 61801-3028 Urbana, Illinois, United States*

**Lijie Liu** − *Key Laboratory of Geographic Information Science (Ministry of Education), School of Geographical Sciences, East China Normal University, 200241 Shanghai, China*

**Yu Li** − *Key Laboratory of Geographic Information Science (Ministry of Education), School of Geographical Sciences, East China Normal University, 200241 Shanghai, China*

**Dong Yang** − *Key Laboratory of Geographic Information Science (Ministry of Education), School of Geographical Sciences, East China Normal University, 200241 Shanghai, China*

**Yingyuan Gao** − *Key Laboratory of Geographic Information Science (Ministry of Education), School of Geographical Sciences, East China Normal University, 200241 Shanghai, China*

**Haowen Tian** − *Key Laboratory of Geographic Information Science (Ministry of Education), School of Geographical Sciences, East China Normal University, 200241 Shanghai, China*

**Rui Cai** − *Key Laboratory of Geographic Information Science (Ministry of Education), School of Geographical Sciences, East China Normal University, 200241 Shanghai, China*

**Zhenlou Chen** − *Key Laboratory of Geographic Information Science (Ministry of Education), School of Geographical Sciences, East China Normal University, 200241 Shanghai, China*

Complete contact information is available at:
https://pubs.acs.org/10.1021/acs.est.1c00114

### Author Contributions

S.C. and D.W. contributed equally to the conception and design of the study and the analysis and interpretation of the data; the manuscript was written by S.C., and D.W. was involved in manuscript revisions. S.C., Y.D., L.L., Y.L., D.Y., Y.G., H.T., and R.C. contributed to the data acquisition. Z.Y. and Z.C. contributed to the revision of the manuscript.

### Notes

The authors declare no competing financial interest.

## ■ REFERENCES

(1) Cole, J. J.; Prairie, Y. T.; Caraco, N. F.; McDowell, W. H.; Tranvik, L. J.; Striegl, R. G.; Duarte, C. M.; Kortelainen, P.; Downing, J. A.; Middelburg, J. J.; Melack, J. Plumbing the global carbon cycle: Integrating inland waters into the terrestrial carbon budget. *Ecosystems* **2007**, *10*, 172−185.

(2) Battin, T. J.; Luyssaert, S.; Kaplan, L. A.; Aufdenkampe, A. K.; Richter, A.; Tranvik, L. J. The boundless carbon cycle. *Nat. Geosci.* **2009**, *2*, 598−600.

(3) Tranvik, L. J.; Downing, J. A.; Cotner, J. B.; Loiselle, S. A.; Striegl, R. G.; Ballatore, T. J.; Dillon, P.; Finlay, K.; Fortino, K.; Knoll, L. B.; Kortelainen, P. L.; Kutser, T.; Larsen, S.; Laurion, I.; Leech, D. M.; McCallister, S. L.; McKnight, D. M.; Melack, J. M.; Overholt, E.; Porter, J. A.; Prairie, Y.; Renwick, W. H.; Roland, F.; Sherman, B. S.; Schindler, D. W.; Sobek, S.; Tremblay, A.; Vanni, M. J.; Verschoor, A. M.; von Wachenfeldt, E.; Weyhenmeyer, G. A. Lakes and reservoirs as regulators of carbon cycling and climate. *Limnol. Oceanogr.* **2009**, *54*, 2298−2314.

(4) Drake, T. W.; Raymond, P. A.; Spencer, R. G. M. Terrestrial carbon inputs to inland waters: A current synthesis of estimates and uncertainty. *Limnol. Oceanogr. Lett.* **2017**, *3*, 132−142.

(5) Kirschke, S.; Bousquet, P.; Ciais, P.; Saunois, M.; Canadell, J. G.; Dlugokencky, E. J.; Bergamaschi, P.; Bergmann, D.; Blake, D. R.; Bruhwiler, L.; Cameron-Smith, P.; Castaldi, S.; Chevallier, F.; Feng, L.; Fraser, A.; Heimann, M.; Hodson, E. L.; Houweling, S.; Josse, B.; Fraser, P. J.; Krummel, P. B.; Lamarque, J.-F.; Langenfelds, R. L.; Le Quéré, C.; Naik, V.; O'Doherty, S.; Palmer, P. I.; Pison, I.; Plummer, D.; Poulter, B.; Prinn, R. G.; Rigby, M.; Ringeval, B.; Santini, M.; Schmidt, M.; Shindell, D. T.; Simpson, I. J.; Spahni, R.; Steele, L. P.; Strode, S. A.; Sudo, K.; Szopa, S.; van der Werf, G. R.; Voulgarakis, A.; van Weele, M.; Weiss, R. F.; Williams, J. E.; Zeng, G. Three decades of global methane sources and sinks. *Nat. Geosci.* **2013**, *6*, 813−823.

(6) Raymond, P. A.; Hartmann, J.; Lauerwald, R.; Sobek, S.; McDonald, C.; Hoover, M.; Butman, D.; Striegl, R.; Mayorga, E.; Humborg, C.; Kortelainen, P.; Dürr, H.; Meybeck, M.; Ciais, P.; Guth, P. Global carbon dioxide emissions from inland waters. *Nature* **2013**, *503*, 355−359.

(7) Davidson, T. A.; Audet, J.; Svenning, J.-C.; Lauridsen, T. L.; Søndergaard, M.; Landkildehus, F.; Larsen, S. E.; Jeppesen, E. Eutrophication effects on greenhouse gas fluxes from shallow-lake mesocosms override those of climate warming. *Global Change Biol.* **2015**, *21*, 4449−4463.

(8) Bastviken, D.; Cole, J. J.; Pace, M. L.; Van de Bogert, M. C. Fates of methane from different lake habitats: Connecting whole-lake budgets and CH4 emissions. *J. Geophys. Res.: Biogeosci.* **2008**, *113*, G02024.

(9) IPCC. *Climate Change 2013: The Physical Science Basis.* Stocker, T. F., Qin, D., Plattner, G.-K., Tignor, M., Allen, S. K., Boschung, J., Nauels, A., Xia, Y., Bex, V., Midgley, P. M., Eds.; Cambridge University Press: Cambridge, United Kingdom and New York, 2013.

(10) Trimmer, M.; Grey, J.; Heppell, C. M.; Hildrew, A. G.; Lansdown, K.; Stahl, H.; Yvon-Durocher, G. River bed carbon and nitrogen cycling: State of play and some new directions. *Sci. Total Environ.* **2012**, *434*, 143−158.

(11) Bastviken, D.; Tranvik, L. J.; Downing, J. A.; Crill, P. M.; Enrich-Prast, A. Freshwater methane emissions offset the continental carbon sink. *Science* **2011**, *331*, 50.

(12) Sawakuchi, H. O.; Bastviken, D.; Sawakuchi, A. O.; Krusche, A. V.; Ballester, M. V. R.; Richey, J. E. Methane emissions from Amazonian Rivers and their contribution to the global methane budget. *Global Change Biol.* **2014**, *20*, 2829−2840.

(13) Borges, A. V.; Darchambeau, F.; Teodoru, C. R.; Marwick, T. R.; Tamooh, F.; Geeraert, N.; Omengo, F. O.; Guérin, F.; Lambert, T.; Morana, C.; Okuku, E.; Bouillon, S. Globally significant greenhouse-gas emissions from African inland waters. *Nat. Geosci.* **2015**, *8*, 637−642.

(14) Stanley, E. H.; Casson, N. J.; Christel, S. T.; Crawford, J. T.; Loken, L. C.; Oliver, S. K. The ecology of methane in streams and rivers: Patterns, controls, and global significance. *Ecol. Monogr.* **2016**, *86*, 146−171.

(15) Wuebbles, D.; Hayhoe, K. Atmospheric methane and global change. *Earth-Sci. Rev.* **2002**, *57*, 177−210.

(16) Garnier, J.; Vilain, G.; Silvestre, M.; Billen, G.; Jehanno, S.; Poirier, D.; Martinez, A.; Decuq, C.; Cellier, P.; Abril, G. Budget of methane emissions from soils, livestock and the river network at the regional scale of the Seine basin (France). *Biogeochemistry* **2013**, *116*, 199−214.

(17) Yu, Z.; Wang, D.; Li, Y.; Deng, H.; Hu, B.; Ye, M.; Zhou, X.; Da, L.; Chen, Z.; Xu, S. Carbon dioxide and methane dynamics in a human-dominated lowland coastal river network (Shanghai, China). *J. Geophys. Res.: Biogeosci.* **2017**, *122*, 1738−1758.

(18) Martinez-Cruz, K.; Gonzalez-Valencia, R.; Sepulveda-Jauregui, A.; Plascencia-Hernandez, F.; Belmonte-Izquierdo, Y.; Thalasso, F. Methane emission from aquatic ecosystems of Mexico City. *Aquat. Sci.* **2017**, *79*, 159−169.

(19) Wang, X.; He, Y.; Chen, H.; Yuan, X.; Peng, C.; Yue, J.; Zhang, Q.; Zhou, L. CH4 concentrations and fluxes in a subtropical metropolitan river network: Watershed urbanization impacts and environmental controls. *Sci. Total Environ.* **2018**, *622−623*, 1079−1089.

(20) Wang, R.; Zhang, H.; Zhang, W.; Zheng, X.; Butterbach-Bahl, K.; Li, S.; Han, S. An urban polluted river as a significant hotspot for water-atmosphere exchange of CH4 and N2O. *Environ. Pollut.* **2020**, *264*, 114770.

(21) Ortega, S. H.; González-Quijano, C. R.; Casper, P.; Singer, G. A.; Gessner, M. O. Methane emissions from contrasting urban freshwaters: rates, drivers, and a whole-city footprint. *Global Change Biol.* **2019**, *25*, 4234−4243.

(22) Wang, G.; Xia, X.; Liu, S.; Zhang, L.; Zhang, S.; Wang, J.; Xi, N.; Zhang, Q. Intense methane ebullition from urban inland waters and its significant contribution to greenhouse gas emissions. *Water Res.* **2021**, *189*, 116654.

(23) Beaulieu, J. J.; DelSontro, T.; Downing, J. A. Eutrophication will increase methane emissions from lakes and impoundments during the 21st century. *Nat. Commun.* **2019**, *10*, 3−7.

(24) Baulch, H. M.; Dillon, P. J.; Maranger, R.; Schiff, S. L. Diffusive and ebullitive transport of methane and nitrous oxide from streams: Are bubble-mediated fluxes important? *J. Geophys. Res.: Biogeosci.* **2011**, *116*, G04028.

(25) Prairie, Y.; del Giorgio, P. A new pathway of freshwater methane emissions and the putative importance of microbubbles. *Inland Waters* **2013**, *3*, 311−320.

(26) DelSontro, T.; Boutet, L.; St-Pierre, A.; del Giorgio, P. A.; Prairie, Y. T. Methane ebullition and diffusion from northern ponds and lakes regulated by the interaction between temperature and system productivity. *Limnol. Oceanogr.* **2016**, *61*, S62−S77.

(27) Ostrovsky, I.; Mcginnis, D. F.; Lapidus, L.; Eckert, W. Quantifying gas ebullition with echosounder: The role of methane transport by bubbles in a medium-sized lake. *Limnol. Oceanogr.* **2008**, *6*, 105−118.

(28) Delsontro, T.; Kunz, M. J.; Kempter, T.; Wüest, A.; Wehrli, B.; Senn, D. B. Spatial heterogeneity of methane ebullition in a large tropical reservoir. *Environ. Sci. Technol.* **2011**, *45*, 9866−9873.

(29) Delsontro, T.; McGinnis, D. F.; Wehrli, B.; Ostrovsky, I. Size does matter: Importance of large bubbles and small-scale hot spots for methane transport. *Environ. Sci. Technol.* **2015**, *49*, 1268−1276.

(30) Bastviken, D.; Cole, J.; Pace, M.; Tranvik, L. Methane emissions from lakes: Dependence of lake characteristics, two regional assessments, and a global estimate. *Global Biogeochem. Cycles* **2004**, *18*, a−n.

(31) Wilcock, R. J.; Sorrell, B. K. Emissions of Greenhouse Gases CH4 and N2O from Low-gradient Streams in Agriculturally Developed Catchments. *Water Air Soil Pollut.* **2008**, *188*, 155−170.

(32) Crawford, J. T.; Stanley, E. H.; Spawn, S. A.; Finlay, J. C.; Loken, L. C.; Striegl, R. G. Ebullitive methane emissions from oxygenated wetland streams. *Global Change Biol.* **2014**, *20*, 3408−3422.

(33) Zhang, L.; Xia, X.; Liu, S.; Zhang, S.; Li, S.; Wang, J.; Wang, G.; Gao, H.; Zhang, Z.; Wang, Q.; Wen, W.; Liu, R.; Yang, Z.; Stanley, E. H.; Raymond, P. A. Significant methane ebullition from alpine permafrost rivers on the East Qinghai-Tibet Plateau. *Nat. Geosci.* **2020**, *13*, 349−354.

(34) Grinham, A.; Dunbabin, M.; Gale, D.; Udy, J. Quantification of ebullitive and diffusive methane release to atmosphere from a water storage. *Atmos. Environ.* **2011**, *45*, 7166−7173.

(35) Sobek, S.; Delsontro, T.; Wongfun, N.; Wehrli, B. Extreme organic carbon burial fuels intense methane bubbling in a temperate reservoir. *Geophys. Res. Lett.* **2012**, *39*, L01401.

(36) Zhang, W.; Xiao, S.; Xie, H.; Liu, J.; Lei, D.; Lorke, A. Diel and seasonal variability of methane emissions from a shallow and eutrophic pond. *Biogeosci. Discuss.* **2020**, 1−40.

(37) Zhu, Y.; Purdy, K. J.; Eyice, Ö.; Shen, L.; Harpenslager, S. F.; Yvon-Durocher, G.; Dumbrell, A. J.; Trimmer, M. Disproportionate increase in freshwater methane emissions induced by experimental warming. *Nat. Clim. Change* **2020**, *10*, 685−690.

(38) Wilkinson, J.; Maeck, A.; Alshboul, Z.; Lorke, A. Continuous seasonal river ebullition measurements linked to sediment methane formation. *Environ. Sci. Technol.* **2015**, *49*, 13121−13129.

(39) Sepulveda-Jauregui, A.; Hoyos-Santillan, J.; Martinez-Cruz, K.; Walter Anthony, K. M.; Casper, P.; Belmonte-Izquierdo, Y.; Thalasso, F. Eutrophication exacerbates the impact of climate warming on lake methane emission. *Sci. Total Environ.* **2018**, *636*, 411−419.

(40) Comer-Warner, S. A.; Romeijn, P.; Gooddy, D. C.; Ullah, S.; Kettridge, N.; Marchant, B.; Hannah, D. M.; Krause, S. Thermal sensitivity of CO2 and CH4 emissions varies with streambed sediment properties. *Nat. Commun.* **2018**, *9*, 2803.

(41) Marcon, L.; Bleninger, T.; Männich, M.; Hilgert, S. High-frequency measurements of gas ebullition in a Brazilian subtropical reservoir-identification of relevant triggers and seasonal patterns. *Environ. Monit. Assess.* **2019**, *191*, 357.

(42) Liu, K.; Su, H.; Zhang, L.; Yang, H.; Zhang, R.; Li, X. Analysis of the urban heat island effect in Shijiazhuang, China using satellite and airborne data. *Remote Sens.* **2015**, *7*, 4804−4833.

(43) Zhou, Y.; Zhou, L.; Zhang, Y.; Garcia de Souza, J.; Podgorski, D. C.; Spencer, R. G. M.; Jeppesen, E.; Davidson, T. A. Autochthonous dissolved organic matter potentially fuels methane ebullition from experimental lakes. *Water Res.* **2019**, *166*, 115048.

(44) Aben, R. C. H.; Barros, N.; Van Donk, E.; Frenken, T.; Hilt, S.; Kazanjian, G.; Lamers, L. P. M.; Peeters, E. T. H. M.; Roelofs, J. G. M.; de Senerpont Domis, L. N.; Stephan, S.; Velthuis, M.; Van de Waal, D. B.; Wik, M.; Thornton, B. F.; Wilkinson, J.; DelSontro, T.; Kosten, S. Cross continental increase in methane ebullition under climate change. *Nat. Commun.* **2017**, *8*, 1682.

(45) Wik, M.; Crill, P. M.; Varner, R. K.; Bastviken, D. Multiyear measurements of ebullitive methane flux from three subarctic lakes. *J. Geophys. Res.: Biogeosci.* **2013**, *118*, 1307−1321.

(46) Cole, J. J.; Caraco, N. F. Atmospheric exchange of carbon dioxide in a low-wind oligotrophic lake measured by the addition of SF6. *Limnol. Oceanogr.* **1998**, *43*, 647−656.

(47) Vachon, D.; Prairie, Y. T.; Cole, J. J. The relationship between near-surface turbulence and gas transfer velocity in freshwater systems and its implications for floating chamber measurements of gas exchange. *Limnol. Oceanogr.* **2010**, *55*, 1723−1732.

(48) Schubert, C. J.; Diem, T.; Eugster, W. Methane emissions from a small wind shielded lake determined by eddy covariance, flux chambers, anchored funnels, and boundary model calculations: A comparison. *Environ. Sci. Technol.* **2012**, *46*, 4515−4522.

(49) Erkkilä, K.-M.; Ojala, A.; Bastviken, D.; Biermann, T.; Heiskanen, J. J.; Lindroth, A.; Peltola, O.; Rantakari, M.; Vesala, T.; Mammarella, I. Methane and carbon dioxide fluxes over a lake: Comparison between eddy covariance, floating chambers and boundary layer method. *Biogeosciences* **2018**, *15*, 429−445.

(50) Liss, P. S.; Slater, P. G. Flux of gases across the air-sea interface. *Nature* **1974**, *247*, 181−184.

(51) Raymond, P. A.; Cole, J. J. Gas exchange in rivers and estuaries: choosing a gas transfer velocity. *Estuaries* **2001**, *24*, 312−317.

(52) Casper, P.; Maberly, S. C.; Hall, G. H.; Finlay, B. J. Fluxes of methane and carbon dioxide from a small productive lake to the atmosphere. *Biogeochemistry* **2000**, *49*, 1−19.

(53) Comer-Warner, S. A.; Gooddy, D. C.; Ullah, S.; Glover, L.; Percival, A.; Kettridge, N.; Krause, S. Seasonal variability of sediment controls of carbon cycling in an agricultural stream. *Sci. Total Environ.* **2019**, *688*, 732−741.

(54) Joyce, J.; Jewell, P. W. Physical controls on methane ebullition from reservoirs and lakes. *Environ. Eng. Geosci.* **2003**, *9*, 167−178.

(55) Maeck, A.; Delsontro, T.; McGinnis, D. F.; Fischer, H.; Flury, S.; Schmidt, M.; Fietzek, P.; Lorke, A. Sediment trapping by dams creates methane emission hot spots. *Environ. Sci. Technol.* **2013**, *47*, 8130−8137.

(56) Wang, D.; Chen, Z.; Sun, W.; Hu, B.; Xu, S. Methane and nitrous oxide concentration and emission flux of Yangtze Delta plain river net. *Sci. China, Ser. B: Chem.* **2009**, *52*, 652−661.

(57) Campeau, A.; del Giorgio, P. A. Patterns in CH4and CO2concentrations across boreal rivers: Major drivers and implications for fluvial greenhouse emissions under climate change scenarios. *Global Change Biol.* **2014**, *20*, 1075−1088.

(58) Striegl, R. G.; Dornblaser, M. M.; McDonald, C. P.; Rover, J. R.; Stets, E. G. Carbon dioxide and methane emissions from the Yukon river system. *Global Biogeochem. Cycles* **2012**, *26*, GB0E05.

(59) Teodoru, C. R.; Nyoni, F. C.; Borges, A. V.; Darchambeau, F.; Nyambe, I.; Bouillon, S. Dynamics of greenhouse gases (CO2, CH4, N2O) along the Zambezi River and major tributaries, and their importance in the riverine carbon budget. *Biogeosciences* **2015**, *12*, 2431−2453.

(60) Hosen, J. D.; McDonough, O. T.; Febria, C. M.; Palmer, M. A. Dissolved organic matter quality and bioavailability changes across an urbanization gradient in headwater streams. *Environ. Sci. Technol.* **2014**, *48*, 7817−7824.

(61) Davidson, T. A.; Audet, J.; Jeppesen, E.; Landkildehus, F.; Lauridsen, T. L.; Søndergaard, M.; Syväranta, J. Synergy between nutrients and warming enhances methane ebullition from experimental lakes. *Nat. Clim. Change* **2018**, *8*, 156−160.

(62) Emilson, E. J. S.; Carson, M. A.; Yakimovich, K. M.; Osterholz, H.; Dittmar, T.; Gunn, J. M.; Mykytczuk, N. C. S.; Basiliko, N.; Tanentzap, A. J. Climate-driven shifts in sediment chemistry enhance methane production in northern lakes. *Nat. Commun.* **2018**, *9*, 1801.

(63) Maeck, A.; Hofmann, H.; Lorke, A. Pumping methane out of aquatic sediments mechanisms that affect the temporal dynamics of ebullition. *Biogeosciences* **2013**, *10*, 18687−18722.

(64) Wik, M.; Thorton, B. F.; Bastviken, D.; MacIntyre, S.; Varner, R. K.; Crill, P. M. Energy input is primary controller of methane bubbling in subarctic lakes. *Geophys. Res. Lett.* **2014**, *41*, 555−560.

(65) McGinnis, D. F.; Greinert, J.; Artemov, Y.; Beaubien, S. E.; Wüest, A. Fate of rising methane bubbles in stratified waters: How much methane reaches the atmosphere? *J. Geophys. Res.: Oceans* **2006**, *111*, 111.

(66) Downing, J. A.; Cole, J. J.; Middelburg, J. J.; Striegl, R. G.; Duarte, C. M.; Kortelainen, P.; Prairie, Y. T.; Laube, K. A. Sediment organic carbon burial in agriculturally eutrophic impoundments over the last century. *Global Biogeochem. Cycles* **2008**, *22*, GB1018.

(67) West, W. E.; Coloso, J. J.; Jones, S. E. Effects of algal and terrestrial carbon on methane production rates and methanogen community structure in a temperate lake sediment. *Freshw. Biol.* **2012**, *57*, 949−955.

(68) Anderson, N. J.; Bennion, H.; Lotter, A. F. Lake eutrophication and its implications for organic carbon sequestration in Europe. *Global Change Biol.* **2014**, *20*, 2741−2751.

(69) Al-Haj, A. N.; Fulweiler, R. W. A synthesis of methane emissions from shallow vegetated coastal ecosystems. *Global Change Biol.* **2020**, *26*, 2988−3005.

(70) Sinha, E.; Michalak, A. M.; Balaji, V. Eutrophication will increase during the 21st century as a result of precipitation changes. *Science* **2017**, *357*, 405−408.

(71) Fuchs, A.; Lyautey, E.; Montuelle, B.; Casper, P. Effects of increasing temperatures on methane concentrations and methanogenesis during experimental incubation of sediments from oligotrophic and mesotrophic lakes. *J. Geophys. Res.: Biogeosci.* **2016**, *121*, 1394−1406.

(72) Yvon-Durocher, G.; Allen, A. P.; Bastviken, D.; Conrad, R.; Gudasz, C.; St-Pierre, A.; Thanh-Duc, N.; Del Giorgio, P. A. Methane

fluxes show consistent temperature dependence across microbial to ecosystem scales. *Nature* **2014**, *507*, 488−491.

(73) Cole, J. J.; Bade, D. L.; Bastviken, D.; Pace, M. L.; Van de Bogert, M. Multiple approaches to estimating air-water gas exchange in small lakes. *Limnol. Oceanogr.* **2010**, *8*, 285−293.

(74) Poindexter, C. M.; Baldocchi, D. D.; Matthes, J. H.; Knox, S. H.; Variano, E. A. The contribution of an overlooked transport process to a wetland's methane emissions. *Geophys. Res. Lett.* **2016**, *43*, 6276−6284.

(75) Delsontro, T.; Kunz, M. J.; Kempter, T.; Wüest, A.; Wehrli, B.; Senn, D. B. Spatial heterogeneity of methane ebullition in a large tropical reservoir. *Environ. Sci. Technol.* **2011**, *45*, 9866−9873.